Automotive Science and Engineering, Vol. 16, No. 1, (2026), 4966-4979

Iran University of Science and Technology

Automotive Science and Engineering

Journal Homepage: ase.iust.ac.ir

ISSN: 2008-9899

A Numerical Investigation of Inter-Vehicle Spacing on Aerodynamic Drag Using a Two-Dimensional Ahmed Body Model

Ata Ahmadabadi[1], Hamed Chehrmonavari[1], Amirhasan Kakaee[1*]

[1] School of Automotive Engineering, Iran University of Science and Technology, Narmak, Tehran, Iran

ARTICLE INFO

Article history:
Received : 3 Aug 2025
Accepted: 17 Feb 2026
Published: 4 Mar 2026

Keywords:
Ahmed Body
Inter-Vehicle Spacing
Drag Coefficient
Wake Interaction
Y^+ distribution
CFD

A B S T R A C T

This study employs two-dimensional CFD simulations to analyze how rear slant angle and inter-vehicle spacing dictate aerodynamic drag in a tandem Ahmed body configuration. We systematically evaluated slant angles from 15° to 45° and longitudinal spacings from X/L = 0.1 to 0.5. The results delineate three distinct aerodynamic regimes for the trailing vehicle: a drafting zone at close distances (X/L=0.1) with significantly reduced drag, an interference zone (X/L=0.2-0.3) where drag peaks, and an independence zone (X/L>0.4) where vehicles behave aerodynamically isolated. Furthermore, the model successfully captures the critical drag rise as the slant angle surpasses 30°, a key flow transition. While the simulation over-predicts absolute drag values, which is an expected outcome of the 2D approach, it demonstrates high fidelity in capturing complex trends, providing foundational insights for optimizing vehicle platooning strategies.

1. Introduction

The pursuit of better fuel efficiency and lower environmental impact has turned aerodynamic optimization into a leading challenge in the automotive sector [1,2]. For ground transportation vehicles, being bluff bodies at near ground level, aerodynamic drag is the leading force against motion at high speeds of vehicles, usually contributing more than half of the total propulsion energy [1-3]. This drag is primarily pressure drag, an uncomplicated consequence of flow separation and the existence of a big low-pressure wake zone behind the vehicle [3]. The three-dimensional complex structure of this wake, with enormous separation, recirculation zones, longitudinal trailing vortices, and intricate shear layers, renders prediction of it a focal issue and a major key to unleashing great performance gains [3].

Computational Fluid Dynamics (CFD) became a useful technology for aerodynamic simulation that is able to calculate the most important parameters like drag and lift without exclusive reliance on physical wind tunnels [3]. Advanced numerical and theoretical modeling approaches have also been applied in other thermo-fluid applications, such as the investigation of droplet-scale heat transfer mechanisms and interfacial transport phenomena on hybrid wettability surfaces using dimensionless analysis and numerical frameworks, demonstrating the versatility of CFD-based modeling techniques in complex transport problems [4-6]. Despite its refinements, predictive capability of CFD remains intrinsically dependent on the choice and application of turbulence models, e.g., the widely used RANS-based k-ε and k-ω SST, and the fine resolution of the near-wall flow [7-11]. Among the most important measures of this solution is the non-dimensional wall distance, Y^+, and its distribution; poor meshing in the near-wall region can lead to enormous inaccuracies in the

*Amirhasan Kakaee
Email Address: kakaee_ah@iust.ac.ir
http://doi.org/10.22068/ase.2026.734

"*Automotive Science and Engineering*" is licensed under a Creative Commons Attribution-Noncommercial 4.0 International License.

[Downloaded from rds.iust.ac.ir on 2026-11-15]

[DOI: 10.22068/ase.2026.734]

prediction of crucial phenomena like flow separation, which governs pressure drag [7-11]. The inherent complexity and patented nature of production vehicle shapes have led to the application of simplified models for fundamental research. Leading the rest is the Ahmed body, a reference geometry that well simulates the dominant flow features of a real car, like a classic wake with bi-stability and vortex shedding, and therefore is a most convenient tool for CFD verification and bluff-body aerodynamics investigation [12-13]. Aerodynamic studies of vehicles are increasingly focused on interactive effects, such as those in platooning situations, in which another vehicle's wake can significantly alter the flow field and drag coefficient of a vehicle. Previous research has shown the potential of many flow control strategies. For instance, Abbaspour et al. [14] demonstrated that local boundary layer suction along a 2D Ahmed body can achieve significant drag reduction through wake suppression. Other studies have examined passive devices [15, 16], active methods like

pulsed jets [17, 18], and even closed-loop hybrids [19,20], achieving up to 30% drag reduction [20]. Some of the recent experiments have been investigating the aerodynamic performance of the Ahmed body for the purpose of understanding flow separation, wake behavior, and drag-reduction phenomena. Hung Tran et al. [21] concluded that deflectors produced a maximum drag reduction of 8%, reporting it due to breakdown of separation bubbles and longitudinal vortices transformation. Similarly, Li et al. [22] studied the body in crosswind, with parabolic drag variation vs. yaw angle explained by asymmetric recirculation patterns and pressure non-uniformity. Plumejeau et al. [23] investigated converging steady blowing, which reduced drag up to 3% by eliminating wake bistability, but increasing jet velocities increased drag. Hung et al. [24] in a different paper demonstrated that a slant-mounted deflector reduced low yaw-angle drag by breaking up vortices, but increased it at large yaw angles. Bello-Millán et al. [25] systematically measured yawed drag and demonstrated three regimes of increasing and stabilizing drag. Moscato et al. [25] introduced unsteady flow, which caused 20% oscillations in loads and decreased time-averaged drag compared to steady flow conditions. Finally, Bruneau et al. [27] showed that pulsed jets and porous surfaces could be employed to deflect wake vortices away and prevent them, and that maximum performance is achieved through a combination of both. In conclusion, these papers of [21-27] are developments in wake structure and pressure distribution control that serve as a foundation for the vehicle design optimization through geometric tuning, active blowing, and crosswind control. Table 1 provides a comparative summary of key studies investigating the drag coefficient and related aerodynamic properties of the Ahmed body model. Grounded on this extensive literature, this present research conducts a quantitative study of aerodynamic interference between two Ahmed bodies. The study employs a two-dimensional simulation in ANSYS Fluent to investigate the effect of inter-model spacing on the drag coefficients of both bodies systematically. In this study, we strategically employed a two-dimensional computational model. This approach allows us to distill the complex problem of tandem vehicle aerodynamics down to its fundamental components. By using a 2D simulation, we can isolate the essential interactions between vehicle spacing, slant angle, and wake coupling, without the confounding influence of three-dimensional structures like longitudinal vortices. This clarity is crucial for building a foundational understanding of the flow physics. Furthermore, the computational efficiency of the 2D approach enabled a comprehensive parametric study across multiple spacings and angles with high mesh fidelity,

Table 1: Recent Advances in Ahmed Body Aerodynamic

Ref.	*Authors*	*Focus / Objective*	*Methodology*	*Key Findings*	*Drag Effect*
[21]	Hung Tran *et al.*	Deflector angle effects on Ahmed body aerodynamics	Experimental (luminescent oil-film, pressure, force)	Drag & lift decrease above −5°; max drag reduction 8% at 0°; linked to vortex breakdown	↓ Drag (up to 8%)
[22]	Jinji Li *et al.*	Crosswind influence on 35° slant Ahmed body	Experimental (PIV, force, pressure)	Drag increases between 6°–16° yaw; asymmetric pressure due to distorted wake	↑ Drag with yaw
[23]	Baptiste Plumejeau *et al.*	Converging steady blowing (active control)	Experimental (PIV, pressure, force)	Steady blowing disrupts bistability, −3% drag; high jet ratios increase drag	Mixed (−3% to ↑)
[24]	Hung *et al.*	Slant deflector effects under crosswind	Experimental (pressure, force, skin friction)	Drag ↓ at small yaw (<8°), ↑ at high yaw; lift ↓ overall	↓ Drag (low yaw)
[25]	Bello-Millán *et al.*	Drag dependence on yaw angle	Wind tunnel tests	Three drag regimes with yaw; drag ↑ for β<10°, constant 10°–20°, ↑ again >20°	↑ Drag with yaw
[26]	Moscato *et al.*	Unsteady inflow and oscillating wake effects	Experimental (dynamic force, PIV)	Unsteady flow reduces mean drag/lift; 20% oscillations in instantaneous loads	↓ Mean drag
[27]	Bruneau *et al.*	Active and passive wake control	Analytical & numerical	Pulsed jets + porous surfaces shift vortices, reducing rear pressure drag	↓ Drag (combined control)

[Downloaded from rds.iust.ac.ir on 2026-11-15]

[DOI: 10.22068/ase.2026.734]

establishing a reliable benchmark for future 3D investigations. The specific research aims are to:

- ✓ Establish and validate a high-fidelity CFD method for the Ahmed body using existing experimental data and boundary conditions from reliable sources [12, 29].
- ✓ Quantify the impact of the gap between two Ahmed models on their respective aerodynamic drag forces.
- ✓ Examine the requirements for effective turbulence modeling, of particular interest being the pivotal role of Y^+ value distribution in boundary layer resolution and separation prediction [4-8].
- ✓ Perform a comprehensive study of boundary layer growth and resulting wake flow dynamics.
- ✓ More stringent checks of the simulation predictions against existing experimental and numerical data from the literature to ensure reliability [11, 25-28].

By performing these tasks, this research can provide truthful information on the complex aerodynamic interactions between different bluff bodies, thereby providing valuable information for the creation of efficient vehicle platooning methods and novel drag-reduction technologies.

2. Experimental detail

Introduced in the 1980s by Ahmed et al. [12], the Ahmed body serves as a canonical simplified automotive model for evaluating turbulence models against complex flow geometries. Its design comprises a rounded nose, a central rectangular section, and an adjustable rear slant, enabling systematic analysis of flow separation across various angles (Fig.1). While geometrically simplified, this configuration preserves the essential aerodynamic phenomena present in actual vehicle flows, including the critical wake vortices responsible for dominant pressure drag components. The growing emphasis on aerodynamic optimization in vehicle development necessitates advanced flow control strategies, yet the geometrical complexity of production vehicles complicates systematic validation. The Ahmed body addresses this challenge by providing a benchmark geometry that retains the fundamental flow characteristics—particularly the vortex-driven wake dynamics—within a computationally and experimentally tractable form. As illustrated in Fig. 1, the model's geometry deliberately emphasizes fundamental aerodynamic properties, particularly through the influence of its rear slant angle φ. Aerodynamic coefficients undergo significant transition at φ = 30°, establishing this as the critical slant angle. For configurations with φ ≤ 30° (including the studied 25° case), the flow is characterized by intensifying longitudinal vortex pairs along the rear surface. These structures generate substantial downwash and produce the peak drag condition at φ = 30°, where flow separation occurs at the slant's trailing edge and creates strong localized under-pressure regions [7,32]. Experimental validation was conducted in a low-speed wind tunnel configured with a ¾ open test section (4% blockage ratio).

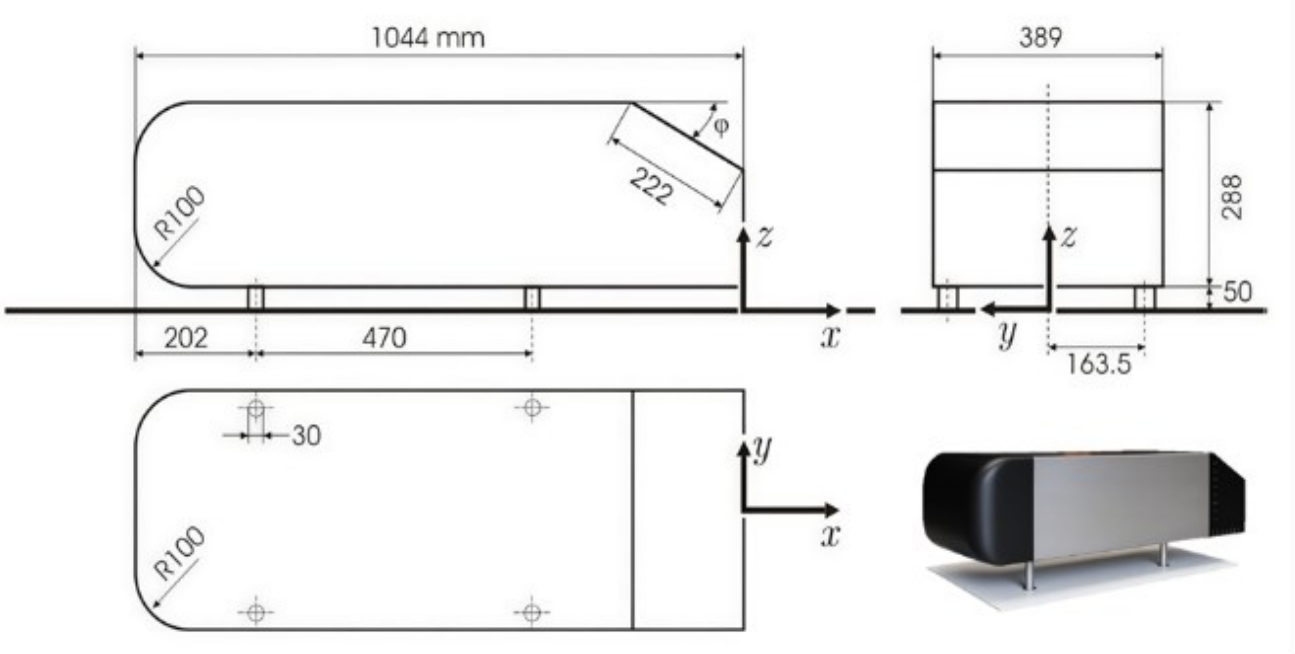


Figure 1. Geometry of the Ahmed body [8]

[Downloaded from rds.iust.ac.ir on 2026-11-15]

[DOI: 10.22068/ase.2026.734]

Measurements were performed at a bulk velocity of 40 m/s under controlled turbulence intensity conditions below 0.25%, with a computerized feedback system maintaining test section stability [34]. This setup enabled detailed velocity profile measurements around the Ahmed body, providing essential validation data for computational models. Table 2 shows the geometric parameters of this model.

Table 2. Geometrical dimension [8,33,34]

Parameter	Value	Unit
Tunnel size	(2 * 1.46) ¾ open test section	m
Length	1.044	m
Height	0.288	m
Front radius	0.1	m
Ground clearance	0.05	m
Slant angle	25°, 35°	degree
Inlet velocity	10, 20, 30, 40	m/s
Yaw angle	B = 0°	degree
Blockage ratio	3.8	%
Cross-sectional area	A = 0.112	m²

3. Numerical model

This study utilizes a two-dimensional CFD analysis in ANSYS to examine how the separation distance between two Ahmed body models affects their aerodynamic drag. The research aims to establish a validated simulation, determine appropriate boundary conditions from literature, analyzing the relationship between spacing and drag, evaluate turbulence model requirements with focus on Y+ distribution, perform boundary layer analysis, and validate results against existing benchmark data.

2.1. Governing Equations

The fluid dynamics are governed by the two-dimensional, steady-state, incompressible forms of the continuity and Reynolds-Averaged Navier-Stokes (RANS) equations. For a steady flow, these equations are expressed as follows [8]:

$$\frac{\partial u}{\partial x}+\frac{\partial v}{\partial y}=0 \qquad (1)$$

The transient flow behavior in the X-direction is governed by the momentum equation, formulated as [8]:

$$\rho u\frac{\partial u}{\partial x}+\rho v\frac{\partial u}{\partial y}=-\frac{\partial \hat{p}}{\partial x}+\mu\left[\frac{\partial^2 u}{\partial x^2}+\frac{\partial^2 u}{\partial y^2}\right] \qquad (2)$$

The Y-direction momentum equation is formulated as [5]:

$$\rho u\frac{\partial v}{\partial x}+\rho v\frac{\partial v}{\partial y}=-\frac{\partial \hat{p}}{\partial y}+\mu\left[\frac{\partial^2 v}{\partial x^2}+\frac{\partial^2 v}{\partial y^2}\right] \qquad (3)$$

In RANS formulation, the instantaneous velocity components are decomposed into mean and fluctuating parts: $'u=u^{-}+u'$ and $v=v^{-}+v'$. Substituting these into the Navier-Stokes equations and time-averaging yields the RANS momentum equations. For the x-direction:

$$\rho\bar{u}\frac{\partial \bar{u}}{\partial x}+\rho\bar{v}\frac{\partial \bar{u}}{\partial y}=-\frac{\partial \bar{p}}{\partial x}+\mu\left(\frac{\partial^2 \bar{u}}{\partial x^2}+\frac{\partial^2 \bar{u}}{\partial y^2}\right)-\rho\left(\frac{\partial \overline{u'u'}}{\partial x}+\frac{\partial \overline{u'v'}}{\partial y}\right) \quad (4)$$

For the y-direction:

$$\rho\bar{u}\frac{\partial \bar{v}}{\partial x}+\rho\bar{v}\frac{\partial \bar{v}}{\partial y}=-\frac{\partial \bar{p}}{\partial y}+\mu\left(\frac{\partial^2 \bar{v}}{\partial x^2}+\frac{\partial^2 \bar{v}}{\partial y^2}\right)-\rho\left(\frac{\partial \overline{u'v'}}{\partial x}+\frac{\partial \overline{v'v'}}{\partial y}\right) \quad (5)$$

The terms $-\rho\overline{u_i'}\overline{u_j'}$ represent the Reynolds stresses, which arise from the fluctuating velocity field and require modeling for closure. In this study, the Realizable k-ε turbulence model is employed to close the RANS equations. This model introduces two additional transport equations: one for turbulent kinetic energy (k) and one for turbulent dissipation rate (ε). The Reynolds stresses are then related to the mean velocity gradients via the Boussinesq hypothesis:

$$-\rho\overline{u_i'}\overline{u_j'}=\mu_t\left(\frac{\partial \bar{u}_i}{\partial x_j}+\frac{\partial \bar{u}_j}{\partial x_i}\right)-\frac{2}{3}\rho k\delta_{ij} \quad (6)$$

where μ_t is the turbulent eddy viscosity, computed as$\mu_t=\rho C_\mu k^2/\varepsilon$, and δ_{ij} is the Kronecker delta. The transport equations for k and ε, along with the model constants, are implemented as per the ANSYS Fluent formulation [8].

3.1. Boundary condition and Mesh Generation

This study investigates the aerodynamic interaction between two Ahmed bodies using Computational Fluid Dynamics (CFD). The

[Downloaded from rds.iust.ac.ir on 2026-11-15]

[DOI: 10.22068/ase.2026.734]

simulations were performed in a virtual wind tunnel measuring 2000 mm by 9000 mm. A lead vehicle was fixed 1000 mm from the inlet, and both models were elevated 50 mm from the floor to simulate ground clearance. Five longitudinal spacings, defined by the ratio X/L = 0.1, 0.2, 0.3, 0.4, and 0.5, were analyzed. The boundary conditions were set to model a controlled flow environment. The tunnel inlet was specified as a velocity inlet with a uniform stream wise velocity of 35 m/s, while the outlet was defined as a pressure outlet. Turbulence was characterized by an intensity of 1.8% and a turbulent viscosity ratio of 10. All vehicle surfaces and the tunnel floor were modeled as stationary no-slip walls to capture viscous effects. The computational domain was discretized in ANSYS Workbench using a patch-conforming algorithm. A structured quad-dominant mesh was selected for this study due to its specific advantages for external aerodynamics. This type of mesh provides superior control over cell alignment with the expected flow direction, which enhances numerical accuracy and convergence. Most importantly, it allows for the creation of highly anisotropic (high aspect ratio) cells immediately adjacent to the vehicle surfaces. These cells are essential for resolving the steep velocity gradients within the boundary layer while maintaining a manageable total cell count. This careful meshing strategy is fundamental for accurately predicting flow separation and the resulting pressure drag. Three key mesh quality criteria were considered for this simulation: skewness, orthogonality, and aspect ratio. Skewness measures cell distortion and alignment with the solution domain; a value closer to zero indicates higher quality, which is especially important for triangular and quadrilateral elements. Orthogonality assesses the perpendicularity of cell faces and their alignment with the flow, where a value closer to one generally denotes a superior mesh. Finally, the Aspect Ratio describes the proportionality of a cell's sides, with a lower value being preferable. For instance, an element with sides of 25 cm and 1 cm has an aspect ratio of 25, indicating a highly stretched, low-quality cell that is unsuitable for accurate simulation. (Fig.2)

A grid independence study was conducted to ensure the numerical accuracy of the CFD results. Four progressively refined meshes, consisting of approximately 60,000, 120,000, 175,973, and 240,000 cells, were tested. The drag coefficient showed a variation of less than 2% between the two finest grids (Fig. 3).

Based on these results, the mesh with 175,973 elements was selected as the final computational grid. This resolution provides a balance between solution accuracy and computational cost, as it yields less than a 2% variation in key outputs, such as pressure drop, compared to finer grids, indicating mesh-independent results. The final discretized model with its boundary conditions is presented in Fig. 4. This framework enables a precise analysis of the flow field and a systematic investigation into how inter-vehicle spacing influences the aerodynamic drag coefficient.

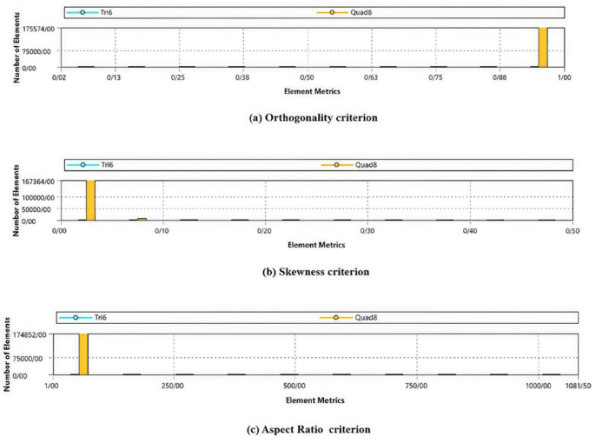


Figure 2. Three main criteria for evaluating network quality in CFD analysis

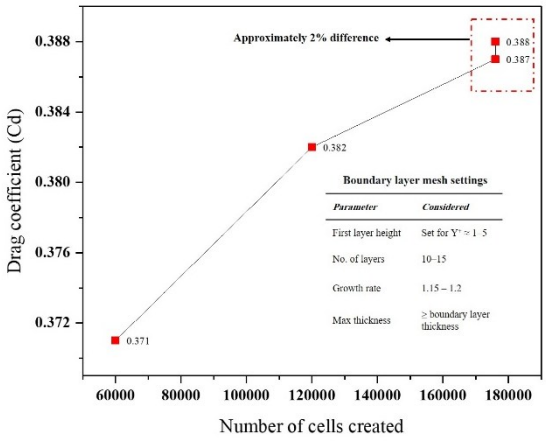


Figure 3. Grid independence test showing convergence of drag coefficient (Cd) with increasing number of mesh elements.

[Downloaded from rds.iust.ac.ir on 2026-11-15]

[DOI: 10.22068/ase.2026.734]

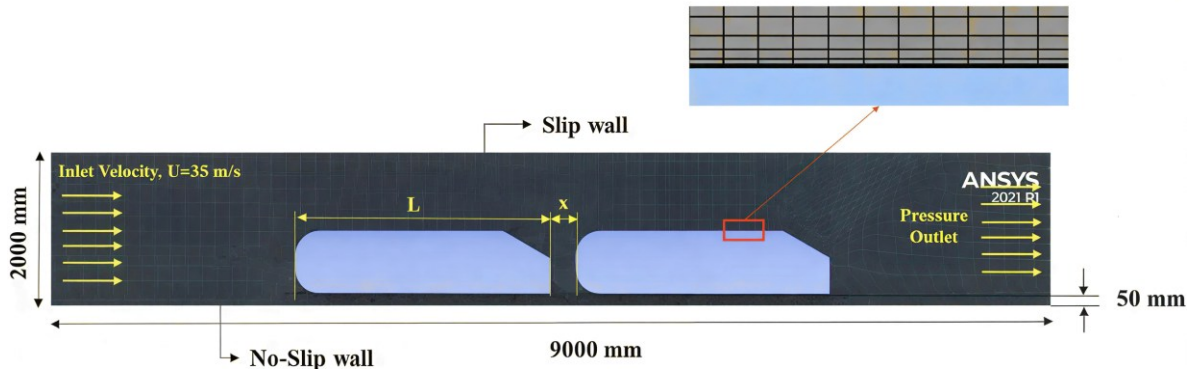


Figure 4. Three main criteria for evaluating network quality in CFD analysis

3.3. Solver Setup

The CFD simulations for this study were conducted using ANSYS Fluent 2021 R2. We employed a two-dimensional, transient, pressure-based solver to model the incompressible flow. The geometry was discretized in ANSYS Workbench, and upon importing, the mesh quality was verified and the domain was scaled to its physical dimensions. To accurately resolve the boundary layer, the Realizable k–ε turbulence model with Enhanced Wall Treatment (EWT) was selected, providing an optimal balance of computational efficiency and resolution for near-wall flow phenomena. The turbulence model constants were set in Table 3. For the solution methods, pressure–velocity coupling was handled using the PISO scheme with skewness correction set to 1 and neighbor correction also set to 1. Spatial discretization was defined with the Green–Gauss cell-based scheme for gradients, PRESTO for pressure, and the QUICK scheme for momentum, turbulent kinetic energy, and turbulent dissipation rate. Solution controls were tuned with appropriate under-relaxation factors to ensure numerical stability and convergence: pressure (0.7), density (1.0), body force (1.0), momentum (0.7), and turbulent kinetic energy (0.7). All flow, turbulence, and energy equations were included in the iterative solution process. The solution initialization was performed from the inlet region, using specified initial values to provide a stable starting point for the simulation. Finally, the numerical calculations were executed for 1000 iterations, with reporting set at every iteration to closely monitor the convergence history (Table 3). Convergence was monitored using scaled residuals for continuity, x-velocity, y-velocity, turbulent kinetic energy (k), and turbulent dissipation rate (ε). The convergence criterion was set such that all residuals fell below 1×10−41×10−4, which is a standard threshold for steady RANS simulations of external aerodynamic flows [8, 32]. In addition to residual monitoring, the drag coefficient (Cd) on both vehicle surfaces was tracked throughout the iterations to ensure it stabilized and showed no significant variation (less than 0.5%) over the final 200 iterations, confirming that a steady-state solution had been achieved.

Table 3. CFD Model Coefficients and Parameters (All simulations were run for 1000 iterations, with convergence assessed based on both residual thresholds and the stabilization of the drag coefficient)

Category	Parameter / Constant	Value / Scheme
Solver Setup	Type	2D, Steady, Incompressible, Double Precision
	Processing	Serial
Turbulence Model	Model	k–ε Enhance Wall Treatment
	C_μ	0.09
	$C_{1\varepsilon}$	1.44
	$C_{2\varepsilon}$	1.92
	σ_k	1.0
	σ_ρ	1.3
Fluid Properties	Air Density (ρ)	1.225 kg/m^3
	Air Viscosity (μ)	1.7894 × 10^{-5} kg/ms
Solid Properties	Aluminum Density (ρ)	2719 kg/m^3
Solution Methods	Pressure–Velocity Coupling	PISO, skewness correction = 1, neighbor correction = 1
	Gradient	Green–Gauss cell-based
	Pressure	PRESTO
	Momentum	QUICK
	Turbulent Kinetic Energy	QUICK
	Turbulent Dissipation Rate	QUICK
Under-Relaxation	Pressure	0.7
	Density	1.0
	Body Force	1.0
	Momentum	0.7
	Turbulent Kinetic Energy	0.7
Run Conditions	Initialization	From inlet region
	Iterations	1000
	Reporting Interval	1
Convergence Criteria	Residual Target	1×10−41×10−4 for all equations
	Drag Coefficient Stability	<0.5% variation over final 200 iterations

[Downloaded from rds.iust.ac.ir on 2026-11-15]

[DOI: 10.22068/ase.2026.734]

3.4. Validation of Simulated Results

The simulation model was validated by comparing its results for the drag coefficient with existing experimental data [18]. This comparison, performed at a rear slant angle of 35° and a speed of 35 m/s, is presented in Table 4 [12] and graphically in Fig. 5. The computational model was validated by comparing the simulated drag coefficient Cd against established experimental data from the literature [21] for the Ahmed body at a velocity of 35 m/s. The validation was performed at two distinct rear slant angles, 25° and 35°, to assess the model's accuracy across different aerodynamic regimes.

The computational model was validated against experimental data for the Ahmed body at 25° and 35° slant angles. As the data indicates, the simulation demonstrates varying levels of agreement with the experimental benchmarks. At the 25° rear slant angle, the model predicted a Cd of 0.31 compared to the experimental value of 0.25, resulting in a percentage error of 19.3%. While this error is non-negligible, it may be considered acceptable in complex aerodynamic simulations where factors like turbulence modeling and numerical dissipation can introduce uncertainties. However, a more significant divergence is observed at the 35° slant angle. Here, the simulation yields a Cd of 0.40 versus the experimental value of 0.2745, leading to a considerably larger percentage error of 32.5%. This level of disagreement suggests a potential limitation in the current computational setup. The high error is attributed to several factors, including the specific turbulence model's inability to accurately capture the complex, unsteady flow separation and reattachment dynamics characteristic of the 35° slant, the fidelity of the mesh in critical regions like the rear base, or differences in the boundary conditions relative to the physical experiment. Therefore, while absolute values at 35° should be interpreted with caution, the model remains valid for investigating the relative trends in aerodynamic drag as a function of inter-vehicle spacing, which is the focus of this study.

In conclusion, while the model provides a first-order approximation, the substantial error at φ = 35° highlights an area where the simulation's predictive capability is limited. This discrepancy warrants further investigation to refine the model, potentially through mesh adaptation, exploration of alternative turbulence models, or a more detailed replication of the experimental conditions. While the simulation over-predicts the absolute drag coefficient at φ = 35°, it successfully captures the critical qualitative trend: a significant increase in drag between the 25° and 35° slant angles. This increase is consistent with experimental observations and is attributed to the known shift in flow topology, specifically the transition from a partially attached flow at 25° to a large, unsteady wake with massive separation at 35°. Therefore, the model is deemed capable of providing valuable insights into the relative aerodynamic behavior and the underlying flow physics, even with the observed quantitative discrepancy.

Table 4. Simulation data validation

Velocity	φ	Simulation C_d	Experiment C_d	% Error
35 m/s	25°	0.31	≅ 0.25	19.3
35 m/s	35°	0.4	0.2745	32.5

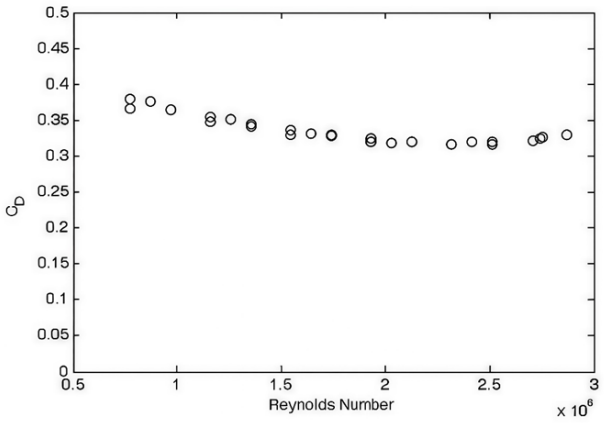


Figure 5. Reynolds number effects on Ahmed model geometry.

4. Simulation of Ahmed body mode at different angle and X/L=0.1, 0.2, 0.3, 0.4, 0.5 (two car)

4.1. Analysis of drag coefficients at the different angles

Our computational analysis reveals a clear aerodynamic trend for the Ahmed body: the drag coefficient increases significantly as the rear slant angle grows from 25° to 45°. This direct relationship, detailed in Fig. 6, is driven by changes in the flow separation behavior. At steeper angles, the flow detaches more readily from the slant edge, generating a larger and more powerful recirculation zone in the wake. This expanded wake creates a substantial low-pressure region at the rear of the body, which dramatically increases the pressure drag component. Since pressure drag dominates the total aerodynamic force on a body, the net result is a sharp rise in the overall drag coefficient [35]. In contrast, at a 15° angle, the flow remains largely attached, resulting

[Downloaded from rds.iust.ac.ir on 2026-11-15]

[DOI: 10.22068/ase.2026.734]

in a comparatively compact wake and the lowest drag observed. While this study provides a definitive link between slant angle and drag force, a complete aerodynamic optimization would require a subsequent analysis of lift.

4.2Analysis of drag coefficients at the distances studied

The effect of inter-vehicle distance on the drag coefficient was quantified by evaluating five longitudinal spacings (X/L). The results, detailed in Fig. 7, reveal a complex aerodynamic interdependence driven by wake interference. For the lead vehicle, the drag coefficient remains relatively stable but exhibits a non-monotonic trend, decreasing from X/L=0.1 to a minimum at X/L=0.2 before gradually increasing again. This suggests a subtle but complex influence from the trailing vehicle's proximity.

The drag on the trailing vehicle is highly sensitive to the distance and demonstrates a classic drafting interaction. At the closest spacing (X/L=0.1), the trailing vehicle experiences its lowest drag coefficient (0.36) as it is fully immersed in the low-pressure wake of the lead vehicle, benefitting from the phenomenon known as drafting [2]. As the distance increases to X/L=0.2, the trailing vehicle begins to emerge from this protective wake, encountering higher-velocity flow which leads to a significant increase in drag. At larger spacings (X/L ≥ 0.3), the drag on the trailing vehicle remains elevated with minor fluctuations as it progressively exits the lead vehicle's wake influence. It is predicted that as the distance extends beyond the tested range, the aerodynamic interaction will diminish further. The drag coefficients for both vehicles will eventually approach those of isolated bodies, signifying aerodynamic independence.

4.3. Analysis of velocity distribution in the investigated distances

Fig. 8 illustrates the velocity contours and streamlines generated by the fluid flow around two Ahmed Body models arranged in tandem at different spacings, quantified by the non-dimensional ratio X/L.

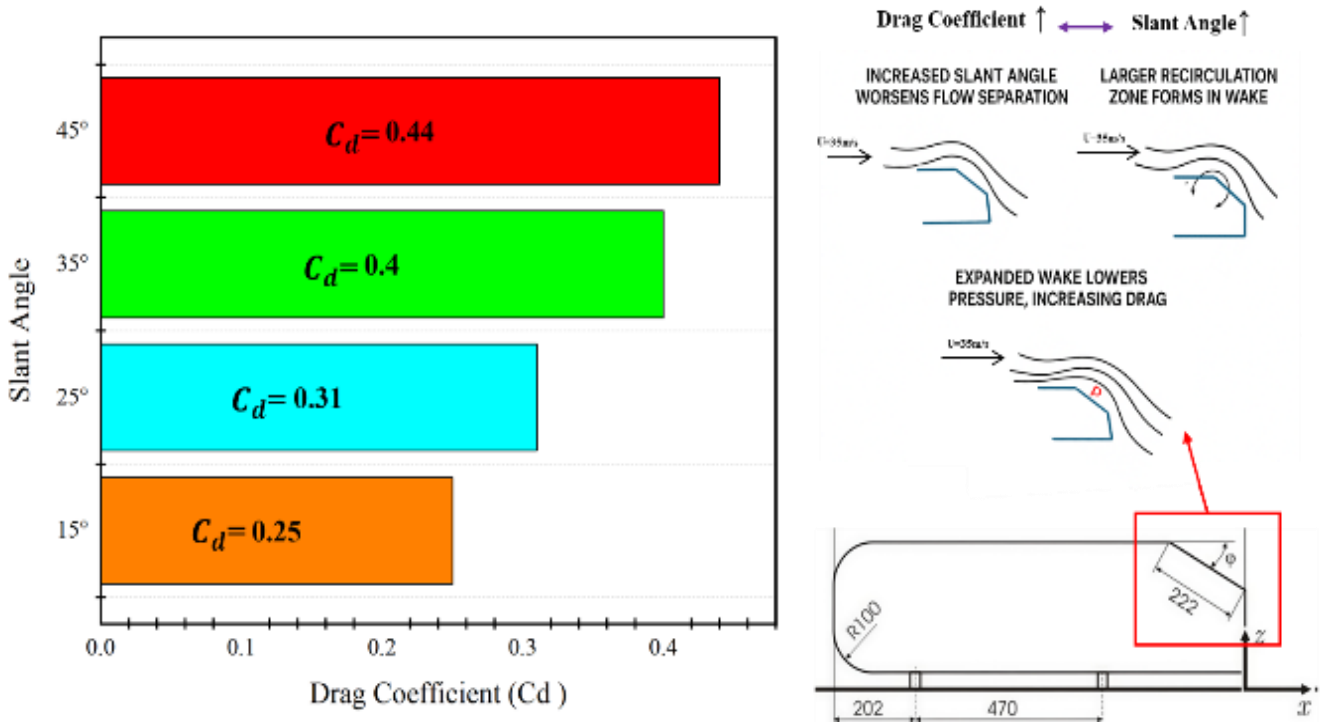


Figure 6. Changes in drag coefficient at different distances: a) Front Car Drag Coefficient, b) Rear Car Drag Coefficient

[Downloaded from rds.iust.ac.ir on 2026-11-15]

[DOI: 10.22068/ase.2026.734]

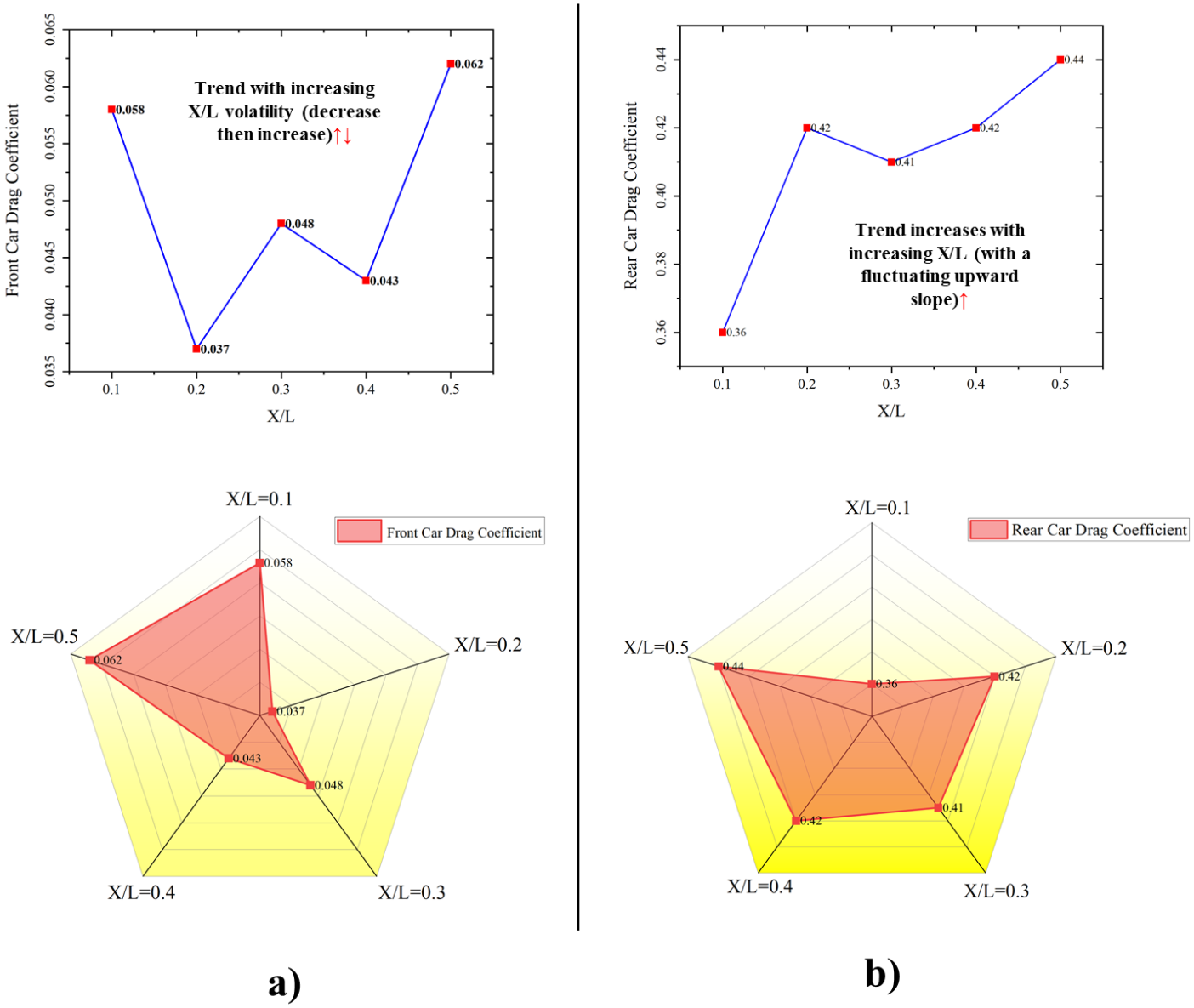


Figure 7. Changes in drag coefficient at different distances: a) Front Car Drag Coefficient, b) Rear Car Drag Coefficient

As detailed in Table 5, an analysis of the velocity contours across all five cases reveals a significant influence on the drag coefficient of the following model. The most favorable condition for drag reduction is observed at a close spacing of X/L = 0.36 (Case a). The contours demonstrate that this spacing allows the trailing model to be fully immersed in the low-momentum wake of the leader while simultaneously leveraging the energy from coherent vortex structures. However, as the gap widens in Cases d and e, the following model exits the protective wake, leading to a progressive loss of the aerodynamic benefit.

[Downloaded from rds.iust.ac.ir on 2026-11-15]

[DOI: 10.22068/ase.2026.734]

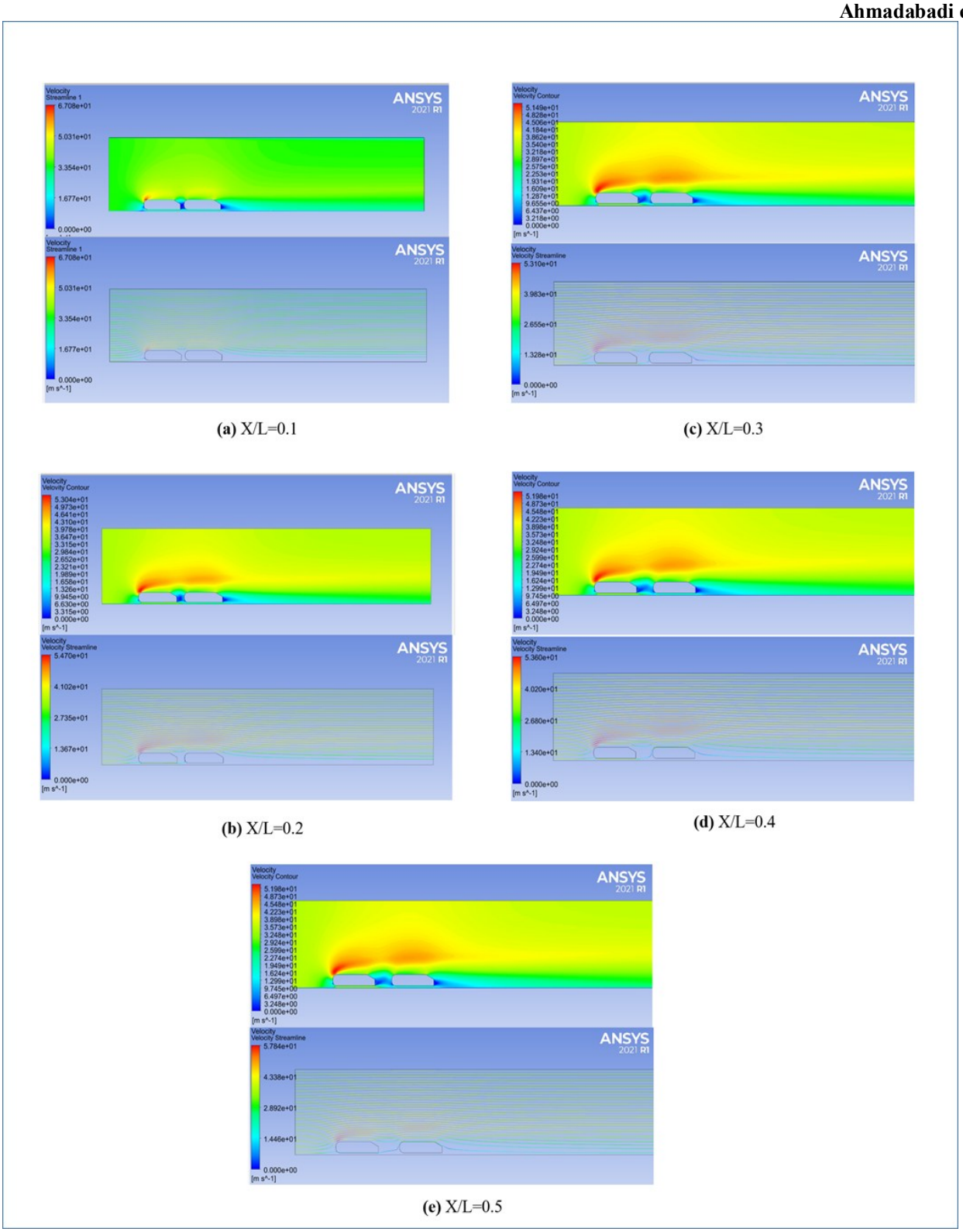


Figure 8. Velocity distribution contours and lines at the distances under investigation

Table 5. Analysis of velocity contours Fig. 6

State	Description of Velocity and Flow Contours	Effect on Drag Force (Second Model)
(a) Very Close	Flow resembles free-stream conditions. Vortices and turbulence almost vanish.	Drag reduction is maximized in this model. Drag approaches the free-flow condition (minimal).
(b) Close	Flow reattaches more effectively; turbulence further decreases. Wake narrows, and base pressure increases.	Noticeable drag reduction. Drag is lower compared to free-flow condition.
(c) Moderate	Flow forms shear layers and vortices but is less intense. Shear layer vortices dominate, and turbulence decreases significantly.	Moderate drag reduction occurs; still higher than free-flow drag, but reduced compared to close distance.
(d) Medium	Flow gradually reattaches with increased velocity. Vortex strength decreases, and base pressure recovery begins.	High drag, but lower than state (a). If velocity increases further, drag reduction begins.
(e) Far	Flow separates completely in the wake region; very high turbulence and low-pressure zone form. Strong recirculation and vortex shedding occur.	Very high drag (drag increases sharply). The second model shows much higher drag compared to the free-flowing fluid.

[Downloaded from rds.iust.ac.ir on 2026-11-15]

[DOI: 10.22068/ase.2026.734]

4.4. Investigating and analyzing the distribution of Y^+ values at different intervals

The non-dimensional wall distance, Y^+, is a critical parameter in Reynolds-Averaged Navier-Stokes (RANS) simulations that dictates the required mesh resolution near a wall to resolve the viscous sublayer. For accurate turbulence modeling, the first cell centroid must be positioned within this sublayer, typically at a Y^+ value of approximately 1 or less. This ensures that the solver can correctly capture the steep velocity gradients in the boundary layer. The value of Y^+ thus serves as a direct measure of mesh quality for wall-bounded flows. In the region below the viscous layer for Y^+ we have:

$$y^+ = u_\tau \frac{y}{v} = \sqrt{\frac{|\tau_\omega|}{\rho}} \frac{\rho}{\mu} y = \sqrt{\rho\,|\tau_\omega|}\,\frac{y}{\mu} \qquad (7)$$

Table 6 delineates the critical influence of the wall-normal resolution (Y+) on the performance of the Enhanced Wall Treatment (EWT) model. The analysis confirms that an optimal Y+ range is paramount for balancing accuracy and computational cost. For EWT, the Y+ parameter dictates the modeling approach in the near-wall region: Y+ < 1: The mesh is excessively refined, fully resolving the viscous sublayer. While this can yield high accuracy, it is computationally expensive and can lead to numerical instability. Ideal Range (Y+ ≈ 1 - 5): This range represents the optimal balance for EWT. The mesh is sufficiently fine to resolve the viscous sublayer directly while maintaining robust and computationally efficient simulations. Y+ > 30: The mesh is too coarse for EWT's intended function, forcing it into a standard wall-function mode. This degrades accuracy and is unsuitable for leveraging the model's enhanced capabilities.

Table 6. Y+ performance of EWT model [36].

Y+ Range	Wall Treatment Behavior	Notes
< 1	Fully resolves viscous sublayer	High mesh density, accurate but costly
~1 - 5	Ideal range for EWT	Good compromise between accuracy and cost
> 30	Wall function regime	Not suitable for EWT

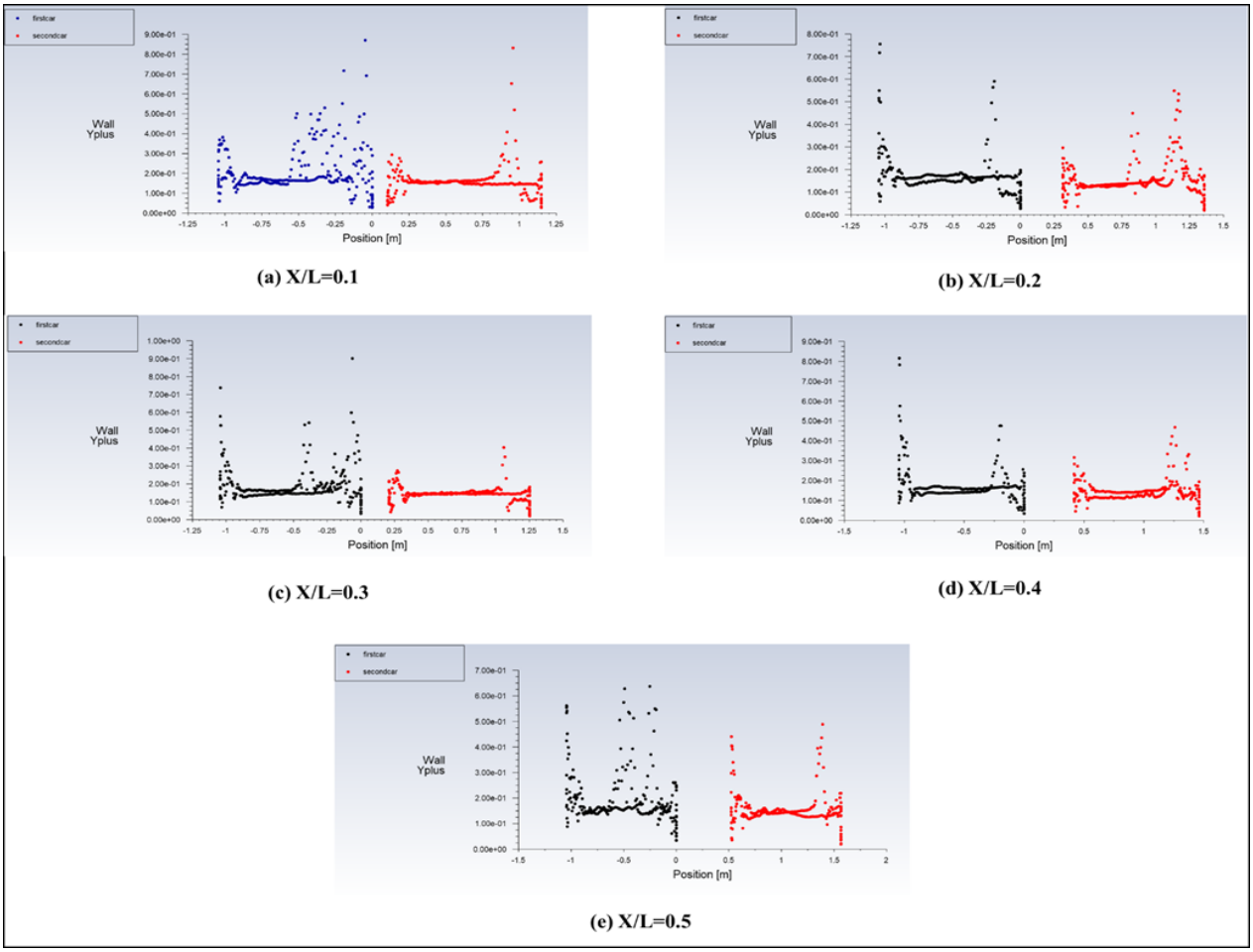


Figure 9. wall Y+ distribution for two Ahmed bodies in tandem at different spacings (X/L = 0.1–0.5)

[Downloaded from rds.iust.ac.ir on 2026-11-15]

[DOI: 10.22068/ase.2026.734]

Fig. 9 presents the wall Y+ distribution for two Ahmed bodies in tandem at different spacings (X/L = 0.1–0.5), simulated using the k–ε turbulence model with Enhanced Wall Treatment. The results show that the leading vehicle exhibits a relatively stable Y+ distribution across all spacings, confirming mesh adequacy for EWT. In contrast, the trailing vehicle is strongly influenced by the wake of the front body, particularly at X/L = 0.1–0.2, where large fluctuations in Y+ occur due to unsteady wake structures and increased turbulence intensity. As the spacing increases to X/L = 0.4–0.5, these disturbances diminish, and the Y+ distribution of the second car approaches that of the front car, though with slightly elevated values, indicating persistent but reduced wake interaction [36].

5. Conclusion

This research provides a comprehensive analysis of the aerodynamic interactions between vehicles in a tandem configuration, revealing how both vehicle geometry and inter-vehicle spacing dictate performance. The study successfully captured the well-known aerodynamic transition of the Ahmed body, confirming a significant drag increase as the rear slant angle surpasses 30 degrees, where airflow shifts from partially attached to fully separated. The investigation into inter-vehicle spacing yielded particularly insightful results, delineating three distinct aerodynamic regimes:

- Drafting Zone (X/L = 0.1): The trailing vehicle experiences a significant drag reduction (Cd = 0.36), achieving its minimum drag coefficient by being fully immersed in the low-pressure wake of the lead vehicle.

- Interference Zone (X/L = 0.2 to 0.3): This regime is characterized by a sharp 16.7% increase in the trailing vehicle's drag as it begins to emerge from the protective wake and encounters higher-velocity, turbulent flow. Concurrently, the lead vehicle exhibits a non-monotonic response, with its drag reaching a minimum at X/L = 0.2.

- Independence Zone (X/L > 0.4): Aerodynamic interaction weakens significantly, and the drag coefficients of both vehicles progressively approach those of isolated bodies, indicating a return to aerodynamic independence.

The research acknowledges its limitations, particularly the use of 2D modeling and the k-ε turbulence model. These constraints, however, provide a clear pathway for future work involving 3D simulations and higher-fidelity turbulence modeling to capture more complex, three-dimensional flow structures.

In conclusion, this work establishes that optimizing aerodynamic efficiency in vehicle convoys requires a dual-focused strategy. The strong dependence of drag on inter-vehicle spacing underscores the critical need to consider both intelligent vehicle design and strategic platoon management. These findings provide a solid foundation for developing more fuel-efficient and sustainable transportation systems.

References

References must be numbered in square brackets and be listed in the list of references in the order that they are referred to in the text. To be compatible with journal format, type in all author names. Do not refer to co-authors as *el al*. New Roman 11 Regular). The complete details of the references will appear in the list of references.

For journal papers, books and conferences papers use the following formats;

[1] M. Koike, T. Nagayoshi, and N. Hamamoto, "Research on drag reduction by vortex generators," *Mitsubishi Motors Technical Review*, No. 16, (2004).

[2] C. H. Bruneau, P. Gilliéron, and I. Mortazavi, "Flow manipulation around the Ahmed body with a rear window using passive strategies," *C. R. Mecanique*, Vol. 335, (2007).

[3] R. S. Khan and S. Umale, "CFD aerodynamic analysis of Ahmed body," *International Journal of Engineering Trends and Technology (IJETT)*, Vol. 18, No. 7, (2014), pp. 301-308.

[4] E. Vatanjoo, E. Aminian, M. Kamali, and H. Saffari, "Theoretical analysis on condensation heat transfer on the hydrophobic–hydrophilic hybrid surfaces with the impact of the Marangoni convection," *Proceedings of the Institution of Mechanical Engineers, Part E: Journal of Process Mechanical Engineering*, Vol. 237, No. 3, (2022), pp. 658-672.

[5] S. Shahlaei, E. Aminian, and H. Saffari, "Numerical study on the effect of Marangoni

[Downloaded from rds.iust.ac.ir on 2026-11-15]

[DOI: 10.22068/ase.2026.734]

convection on condensation heat transfer of hydrophobic and hydrophilic hybrid inclined surfaces," *Proceedings of the Institution of Mechanical Engineers, Part E: Journal of Process Mechanical Engineering*, Vol. 240, No. 1, (2024), pp. 925-941.

[6] A. Babaei, E. Aminian, and H. Saffari, "Numerical study of heat transfer and pressure drop of nanofluids in a combined porous media of hydrophobic and hydrophilic surfaces," *Proceedings of the Institution of Mechanical Engineers, Part A: Journal of Power and Energy*, Vol. 237, No. 6, (2023), pp. 1308-1328.

[7] S. Yongling, W. Guangqiang, and Xieshuo, "Numerical simulation of the external flow field around a bluff car," Shanghai Tongji University, Shanghai, China.

[8] C. B. Rajsinh and R. T. K. Raj, "Numerical investigation of external flow around the ahmed reference body using computational fluid dynamics," *Research Journal of Recent Sciences*, Vol. 1, No. 9, (2012), pp. 1-5.

[9] D. Y. Dhande, "Experimental analysis of aerodynamic aspects of sport utility vehicle," *IJEST*, Vol. 5, No. 7, (2013), pp. 1476-1480.

[10] M. Desai, S. A. Channiwala, and H. J. Nagarsheth, "A comparative assessment of two experimental methods for aerodynamics performance evaluation of car," *Journal of Scientific and Industrial Research*, Vol. 67, (2008), pp. 518-522.

[11] A. I. Heft, T. Indinger, and N. A. Adams, "Introduction of a new realistic generic car model for aerodynamic investigations," *SAE International*, (2012).

[12] S. R. Ahmed, G. Ramm, and G. Faltin, "Some salient features of the time-averaged ground vehicle wake," *SAE Transactions*, Vol. 93, (1984), pp. 473-503.

[13] M. Grandemange, M. Gohlke, and O. Cadot, "Turbulent wake past a three-dimensional blunt body. Part 1. Global modes and bi-stability," *Journal of Fluid Mechanics*, Vol. 722, (2013), pp. 51-84.

[14] M. Abbaspour and M. Jahanmiri, "Two dimensional investigation of the effect of boundary layer suction on drag reduction of a car model," in *9th Annual Iranian Aerospace Society Conference*, The Science and Research Branch-Islamic Azad University, Tehran, Iran, (2010).

[15] A. Evrard, O. Cadot, V. Herbert, D. Ricot, R. Vigneron, and J. Délery, "Fluid force and symmetry breaking modes of a 3D bluff body with a base cavity," *Journal of Fluids and Structures*, Vol. 61, (2016), pp. 99-114.

[16] M. Grandemange, M. Gohlke, and O. Cadot, "Turbulent wake past a three-dimensional blunt body. Part 2. Experimental sensitivity analysis," *Journal of Fluid Mechanics*, Vol. 752, (2014), pp. 439-461.

[17] D. Barros, J. Borée, B. R. Noack, and A. Spohn, "Resonances in the forced turbulent wake past a 3D blunt body," *Physics of Fluids*, Vol. 28, (2016), 065104.

[18] D. J. Parkin, M. C. Thompson, and J. Sheridan, "Numerical analysis of bluff body wakes under periodic open-loop control," *Journal of Fluid Mechanics*, Vol. 739, (2014), pp. 94-123.

[19] R. Li, D. Barros, J. Borée, O. Cadot, B. R. Noack, and L. Cordier, "Feedback control of bimodal wake dynamics," *Experiments in Fluids*, Vol. 57, (2016), 158.

[20] C. H. Bruneau, E. Creusé, D. Depeyras, P. Gilliéron, and I. Mortazavi, "Coupling active and passive techniques to control the flow past the square back Ahmed body," *Computers & Fluids*, Vol. 39, (2010), pp. 1875-1892.

[21] T. H. Tran, M. Hijikuro, M. Anyoji, T. Uchida, T. Nakashima, and K. Shimizu, "Surface flow and aerodynamic drag of Ahmed body with deflectors," *Experimental Thermal and Fluid Science*, Vol. 145, (2023), 110887.

[22] J. Li, Y. Zhang, R. Zhou, Z. Zhang, and G. Wang, "Investigation on aerodynamic force behavior and flow structure of Ahmed body under crosswind," *Experimental Thermal and Fluid Science*, Vol. 166, (2025), 111488.

[23] B. Plumejeau, L. Keirsbulck, J. Basley, M. Lippert, S. Delprat, and W. Abassi, "Drag mitigation by steady blowing and Coanda effect on a square back Ahmed body," *European*

[Downloaded from rds.iust.ac.ir on 2026-11-15]

[DOI: 10.22068/ase.2026.734]

Journal of Mechanics - B/Fluids, Vol. 98, (2023), pp. 80-91.

[24] T. T. Hung, M. Hijikuro, M. Anyoji, T. Uchida, T. Nakashima, and K. Shimizu, "Deflector effect on flow behavior and drag of an Ahmed body under crosswind conditions," *Journal of Wind Engineering and Industrial Aerodynamics*, Vol. 231, (2022), 105238.

[25] F. J. Bello-Millán, T. Mäkelä, L. Parras, C. del Pino, and C. Ferrera, "Experimental study on Ahmed's body drag coefficient for different yaw angles," *Journal of Wind Engineering and Industrial Aerodynamics*, Vol. 157, (2016), pp. 140-144.

[26] G. Moscato and G. P. Romano, "Aerodynamic performances and near wake of an Ahmed body under unsteady flow conditions," *Experimental Thermal and Fluid Science*, Vol. 160, (2025), 111285.

[27] C.-H. Bruneau, E. Creusé, P. Gilliéron, and I. Mortazavi, "Effect of the vortex dynamics on the drag coefficient of a square back Ahmed body: Application to the flow control," *European Journal of Mechanics - B/Fluids*, Vol. 45, (2014), pp. 1-11.

[28] E. Guilmineau, "Computational study of flow around a simplified car body," *Journal of Wind Engineering and Industrial Aerodynamics*, Vol. 96, (2008).

[29] E. Fares, "Unsteady flow simulation of the Ahmed reference body using a lattice Boltzmann approach," *Computers & Fluids*, Vol. 35, (2006), pp. 940-950.

[30] C. Hinterberger, M. Garcia-Villalba, and W. Rodi, "Large eddy simulation of flow around Ahmed body," in *The Aerodynamics of Heavy Vehicles: Trucks, Buses and Trains*, Springer, (2004).

[31] M. Abbaspour and M. Jahanmiri, "Computational study of aerodynamic drag reduction on Ahmed body using active strategies," (2010).

[32] C. M. E. Robinson, "Advanced CFD modeling of road-vehicle aerodynamics," Ph.D. thesis, University of Manchester Institute of Science and Technology, (May 2001).

[33] H. Ahani and M. Uddin, "Modal analyses of flow and aerodynamic characteristics of an idealized ground vehicle using dynamic mode decomposition," *Vehicles*, Vol. 7, No. 2, (2025), 47.

[34] W. Meile, G. Brenn, A. Reppenhagen, B. Lechner, and A. Fuchs, "Experiments and numerical simulations on the aerodynamics of the Ahmed body," *CFD Letters*, Vol. 3, (2011).

[35] A. Kumar, S. Singh, and N. A. Bhalla, "Effect of slant angle variation on the drag force for Ahmed body car model," *Vibroengineering PROCEDIA*, Vol. 29, (Nov. 2019), pp. 153-158.

[36] N. El Gharbi, R. Absi, and A. Benzaoui, "Effect of different near-wall treatments on indoor airflow simulations," *Journal of Applied Fluid Mechanics*, Vol. 5, (2012), pp. 63-70.

[Downloaded from rds.iust.ac.ir on 2026-11-15]

[DOI: 10.22068/ase.2026.734]